Cell Death and Differentiation (2014) 21, 1036–1049

www.nature.com/cdd

LIM kinase-2 induces programmed necrotic neuronal death via dysfunction of DRP1-mediated mitochondrial fission

J-E Kim[1], HJ Ryu[1], MJ Kim[1] and T-C Kang*[,1]

Although the aberrant activation of cell cycle proteins has a critical role in neuronal death, effectors or mediators of cyclin D1/cyclin-dependent kinase 4 (CDK4)-mediated death signal are still unknown. Here, we describe a previously unsuspected role of LIM kinase 2 (LIMK2) in programmed necrotic neuronal death. Downregulation of $p27^{Kip1}$ expression by Rho kinase (ROCK) activation induced cyclin D1/CDK4 expression levels in neurons vulnerable to status epilepticus (SE). Cyclin D1/CDK4 complex subsequently increased LIMK2 expression independent of caspase-3 and receptor interacting protein kinase 1 activity. In turn, upregulated LIMK2 impaired dynamic-related protein-1 (DRP1)-mediated mitochondrial fission without alterations in cofilin phosphorylation/expression and finally resulted in necrotic neuronal death. Inhibition of LIMK2 expression and rescue of DRP1 function attenuated this programmed necrotic neuronal death induced by SE. Therefore, we suggest that the ROCK-$p27^{Kip1}$-cyclin D1/CDK4-LIMK2-DRP1-mediated programmed necrosis may be new therapeutic targets for neuronal death.
Cell Death and Differentiation (2014) **21,** 1036–1049; doi:10.1038/cdd.2014.17; published online 21 February 2014

The cell cycle is essential for a vital process, including proliferation, differentiation and survival of various cells. Cell cycle progression is regulated by two classes of proteins, the cyclins and the cyclin-dependent kinases (CDKs). Among them, cyclin D1 forms a complex with CDK4 and inactivates retinoblastoma protein (Rb) through phosphorylation resulting in activating E2 promoter-binding factor (E2F) family of transcription factors. Active E2F induces various gene transcriptions involving the cell cycle.[1] In post-mitotic neurons, some pathological conditions upregulate cyclin D1/CDK4 complex expression to induce activation of E2F members that contributes to increased transcription of proapoptotic molecules.[2,3] However, it is unclear whether cyclin D1 expression directly induces neuronal death for a number of following reasons. First, due to a time lag between cyclin D1/CDK4 expression and the onset of DNA fragmentation, most cyclin D1-positive neurons show TUNEL negativity.[4,5] Second, cyclin D1 level is unaltered in cultured embryonic neurons following apoptosis induction.[6] Third, Rb phosphorylation is rarely observed *in vivo*,[4] although cyclin D1/CDK4 complex phosphorylates Rb protein in apoptotic cultured neurons.[6] Fourth, cyclin D1 induction following ischemia is associated with regeneration and resistance to apoptosis rather than a mediator of apoptosis.[5,7,8] Fifth, effectors or mediators of cyclin D1/CDK4-mediated death signal are still unknown. Finally, neuronal death induced by various insults is morphologically necrotic rather than apoptotic.[9–12] Therefore, it is likely that some essential factors are missing in the cyclin D/CDK4-mediated neuronal death pathway.

LIM kinases (LIMK1 and LIMK2) phosphorylate cofilin that is a stimulus-responsive mediator of actin dynamics.[13–15] Interestingly, non-phosphorylated cofilin targets mitochondrial membranes in response to apoptotic stimuli for cytochrome *c* release in an actin-independent manner.[16] LIMK2 also translocate into the nucleus, where it mediates suppression of cyclin D1 expression and inhibits G1-to-S phase transition.[17] Thus, LIMKs may involve cyclin D1-mediated neuronal death in actin-dependent or -independent manner. In order to address this hypothesis, we investigated the role of LIMKs in neuronal death induced by status epilepticus (SE, prolonged seizure activity).

Results

LIMK2 overexpression induces necrotic degeneration in CA1 neurons. First, we investigated the alterations in LIMK2 expression and its phosphorylation level following SE.

Western blot studies revealed the gradual upregulation of LIMK2, but not LIMK1, protein following SE ($P<0.05$ *versus* non-SE animals, Figure 1a). LIMK2 mRNA was also increased to 3.8-, 6.1- and 7-fold of the non-SE level at 1, 2 and 3 days after SE, respectively ($P<0.05$, Figure 1b). pLIMK2 S283 and S291 + 293 levels were unaltered, although pLIMK2 T505 level was significantly reduced as compared with non-SE animals ($P<0.05$, Supplementary Figures S1a and b). Cofilin mRNA/protein expression and cofilin phosphorylation were also unaltered by SE (Supplementary Figures S1a–c). LIMK2 knockdown significantly inhibited upregulation of SE-induced

[1]Department of Anatomy and Neurobiology, College of Medicine, Hallym University, Chunchon, Kangwon-Do 200-702, Republic of Korea
*Corresponding author: T-C Kang, Department of Anatomy and Neurobiology, College of Medicine, Hallym University, Chunchon, Kangwon-Do 200-702, Republic of Korea. Tel: +82 33 248 2524; Fax: +82 33 248 2525; E-amil: tckang@hallym.ac.kr
Keywords: $p27^{Kip1}$; cyclin D1/cyclin-dependent kinase 4; LIM kinase 2; dynamic-related protein-1; necrotic neuronal death; seizure
Abbreviations: CDK, cyclin-dependent kinase; Rb, retinoblastoma protein; E2F, E2 promoter-binding factor; LIMK, LIM kinase; SE, status epilepticus; DOX, doxycycline; NFκB, nuclear factor-kappa B; ROCK, Rho kinase; RIP1, receptor interacting protein kinase 1; NEC-1, necrostatin-1; PBS, phosphate-buffered saline; FJB, Fluoro-Jade B; DRP1, dynamic-related protein-1; RALBP1, RALA binding protein 1; HMGB1, high mobility group box 1
Received 01.8.13; revised 09.12.13; accepted 15.1.14; Edited by L Greene; published online 21.2.14

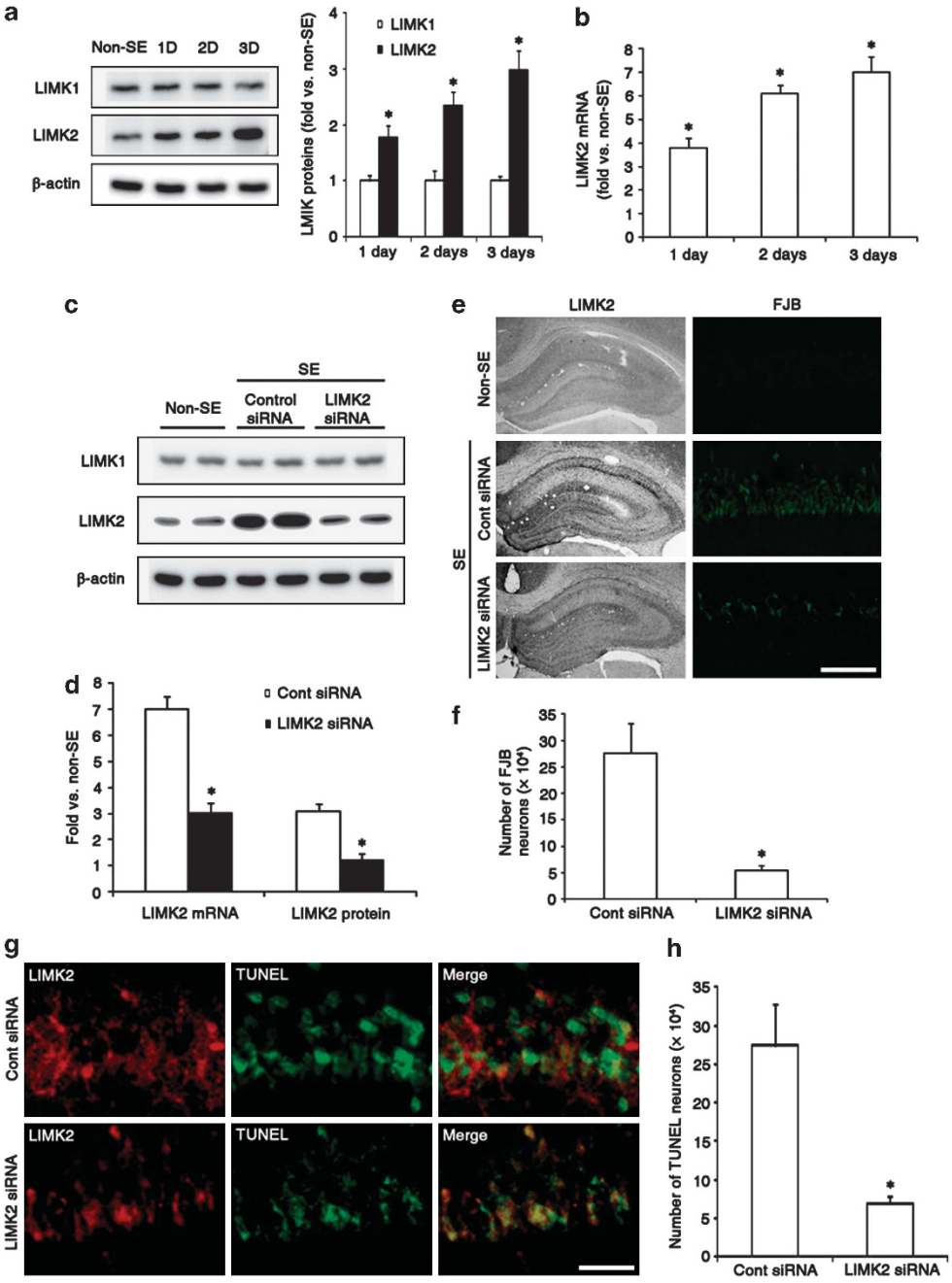

Figure 1 LIMK2-mediated neuronal death following SE. (**a**) Western blotting shows the gradual upregulation of LIMK2 protein level following SE. *$P<0.05$ *versus* non-SE ($n=5$, respectively). (**b**) Quantitative reverse transcriptase-PCR data show that LIMK2 mRNA is increased following SE. *$P<0.05$ *versus* non-SE ($n=5$, respectively). (**c** and **d**) *LIMK2* siRNA significantly inhibits SE-induced LIMK2 mRNA/protein expression levels. *$P<0.05$ *versus* control siRNA ($n=5$, respectively). (**e**) Upregulation of LIMK2 expression is detected in CA1 pyramidal cells. Bar = 400 μm (LIMK2) and 50 μm (FJB). (**f**) *LIMK2* siRNA significantly decreases the number of FJB-positive neurons induced by SE. *$P<0.05$ *versus* control siRNA ($n=5$, respectively). (**g** and **h**) Most LIMK2-positive neurons show TUNEL signals. *LIMK2* siRNA significantly reduces TUNEL signal induced by SE. *$P<0.05$ *versus* control siRNA ($n=5$, respectively). Bar = 12.5 μm

LIMK2 mRNA/protein expression ($P<0.05$ *versus* control siRNA, Figures 1c and d). *LIMK2* siRNA significantly reduced pLIMK2 T505, S283 and S291 + 293 levels following SE ($P<0.05$ *versus* control siRNA, Supplementary Figures S1a and b). However, *LIMK2* siRNA did not affect expression of cofilin mRNA/protein and its phosphorylation as compared with control siRNA (Supplementary Figures S1a–c).

Immunohistochemical data revealed that SE upregulated LIMK2 expression in CA1 pyramidal cells (Figure 1e). Most LIMK2-positive neurons (92%) showed TUNEL signals (Figure 1g). These CA1 neurons showed decrease in phalloidin (a F-actin marker) signal, swollen dendrites with disassembled microtubules and pyknotic nuclei ($P<0.05$ *versus* non-SE animals, Supplementary Figures S1d and e).

Furthermore, high mobility group box 1 (HMGB1) was released from nuclei and finally disappeared in CA1 neurons following SE, although HMGB1 immunoreactivity was detected only in the nuclei in non-SE animals (Supplementary Figures S1f and g). As HMGB1, normally residing in nuclei, translocates to the cytoplasm and/or extracellular space undergoing necrosis but not apoptosis,[18,19] these findings indicate that SE induces necrotic neuronal degeneration rather than apoptosis.

LIMK2 knockdown attenuated the number of Fluoro-Jade B (FJB) and TUNEL-positive neurons induced by SE ($P<0.05$ *versus* control siRNA, Figures 1e–h). *LIMK2* siRNA also prevented the reduction in the phalloidin signal, microtubule disassembly and translocation of HMGB1 to cytoplasm induced by SE ($P<0.05$ *versus* control siRNA, Supplementary figures S1d–g). Taken together, the present data suggest that LIMK2 overexpression may have an important role in necrotic neuronal death independent of cofilin phosphorylation and F-actin contents.

Cyclin D1/CDK4 activation upregulates LIMK2 expression following SE. To elucidate the relationship between cyclin D1/CDK4 complex and LIMK2 expression, we investigate cyclin D1/CDK complex expression profiles in the rat hippocampus following SE.

One day after SE, cyclin D1 mRNA expression was increased 2.5-fold of the non-SE level ($P<0.05$ *versus* non-SE animals, Supplementary Figure S2a). Cyclin D1 mRNA expression was 1.43-fold of the non-SE level 2 days after SE ($P<0.05$ *versus* 1 day after SE, Supplementary Figure S2a). Cyclin D1 protein expression was 3.51- and 2.72-fold of the non-SE level 1 and 2 days after SE, respectively ($P<0.05$ *versus* non-SE animals, Supplementary Figures S2b and c). CDK4 mRNA/protein expression was significantly elevated 1.58–1.75-fold of the non-SE level at 1–2 days after SE ($P<0.05$ *versus* non-SE animals, Supplementary Figures S2a–c). Active caspase-3 was unaltered following SE (Supplementary Figures S2b and c). Cyclin D1 and CDK4 immunoreactivities were obviously visible in CA1 pyramidal cells following SE (Supplementary Figure S2d). One day after SE, 23% of cyclin D1-positive neurons showed LIMK2 expression. Cyclin D1 expression in LIMK2-positive neurons was 0.37-fold of that in LIMK2-negative neurons ($P<0.05$ *versus* LIMK2-negative neurons, Supplementary Figures S2e and f). Two days after SE, only 7% of cyclin D1-positive neurons showed LIMK2 expression. In addition, 11% of TUNEL-positive neurons showed cyclin D1 immunoreactivity (Supplementary Figure S2f).

Consistent with the reported function of LIMK2 as a repressor of cyclin D1 transcriptional induction,[17] *LIMK2* siRNA elevated the expression of cyclin D1 mRNA/protein induced by SE (Figures 2a–d). *LIMK2* siRNA did not affect expression of CDK4 mRNA/protein induced by SE (Figures 2a–c). Flavopiridol (a cyclin D1/CDK4 inhibitor) significantly reduced mRNA/protein expression levels of cyclin D1, CDK4 and LIMK2 (Figures 2e–g) and attenuated SE-induced neuronal death (Figures 2h and i). These findings indicate that LIMK2 may be one of the essential downstream components of cyclin D1/CDK4-mediated neuronal death and that LIMK2 overexpression may be a negative feedback response to inhibit SE-induced cyclin D1 expression.

$p27^{Kip1}$ is a regulator of LIMK2-mediated neuronal death induced by SE. $p27^{Kip1}$ is the best known endogenous CDK inhibitor that binds to the cyclin D1/CDK4 complex.[20] Therefore, we examined the relationship between $p27^{Kip1}$ and LIMK2 expression in SE-induced neuronal death.

SE decreased $p27^{Kip1}$ immunoreactivity in CA1 pyramidal cells vulnerable to SE (Figure 3a). $p27^{Kip1}$ mRNA was decreased to 0.58–0.75-fold of the non-SE level 1–3 days after SE (Figure 3b). $p27^{Kip1}$ protein expression was also reduced to 0.48-fold of the non-SE level 3 days after SE (Figures 3c and d). *LIMK2* siRNA did not prevent down-regulation of $p27^{Kip1}$ expression induced by SE (Figures 3c and d). As doxycycline (DOX) increases $p27^{Kip1}$ gene promoter transactivation via upregulation of cofilin expression,[21,22] we applied DOX to increase $p27^{Kip1}$ expression before SE induction. As expected, DOX significantly increased $p27^{Kip1}$ mRNA/protein expression, cofilin expression, pLIMK2 T505 and pCofilin levels ($P<0.05$ *versus* vehicle, Figures 3e–g). In contrast, DOX prevented upregulation of cyclin D1, CDK4 and LIMK2 mRNA/protein expression induced by SE ($P<0.05$ *versus* vehicle, Figures 3e–g). Immunofluorescence study revealed that DOX inhibited the reduction in $p27^{Kip1}$ expression as well as the induction of cyclin D1 expression in CA1 neurons following SE (Figure 3h). Furthermore, DOX attenuated SE-induced neuronal death ($P<0.05$ *versus* vehicle, Figures 3i and j). These findings indicate that reduced $p27^{Kip1}$ expression may initiate upregulation of LIMK2 expression by cyclin D1 induction following SE.

Rho kinase (ROCK), not NFκB, increases cyclin D1 expression via reduction in $p27^{Kip1}$ expression induced by SE. Nuclear factor-kappa B (NFκB)-mediated signal regulates cyclin D1 and $p27^{Kip1}$ expression.[23,24] Furthermore, p65-Ser536 NFκB phosphorylation is closely related to SE-induced neuronal deaths.[25] Therefore, we investigated the roles of NFκB in cyclin D1 and LIMK2 expression induced by SE.

SN50 (a NFκB inhibitor) treatment did not affect $p27^{Kip1}$, cyclin D1, CDK4 and LIMK2 mRNA/protein expression levels induced by SE (Figures 4a, b and d). SN50 increased LIMK2 T505 (not S283 or S291 + 293) and cofilin phosphorylation ($P<0.05$ *versus* vehicle, Figures 4b and d). However, SN50 did not attenuate SE-induced neuronal death (Figures 4e and f). These findings indicate that NFκB signal may not participate in SE-induced neuronal death, although it may decrease LIMK2 and cofilin phosphorylations by an unknown pathway. Together with the data concerning *LIMK2* siRNA and DOX treatment, our data suggest that cofilin and LIMK2 phosphorylations may not involve neuronal death.

As ROCK activity regulates cyclin D1, $p27^{Kip1}$ and LIMK2 functions,[26] we applied Y-27632 (a ROCK inhibitor) before SE induction to validate the roles of ROCK in SE-induced neuronal death. Y-27632 infusion increased expression of $p27^{Kip1}$ mRNA/protein following SE ($P<0.05$ *versus* vehicle, Figures 4a, c and d). In contrast, Y-27632 reduced the

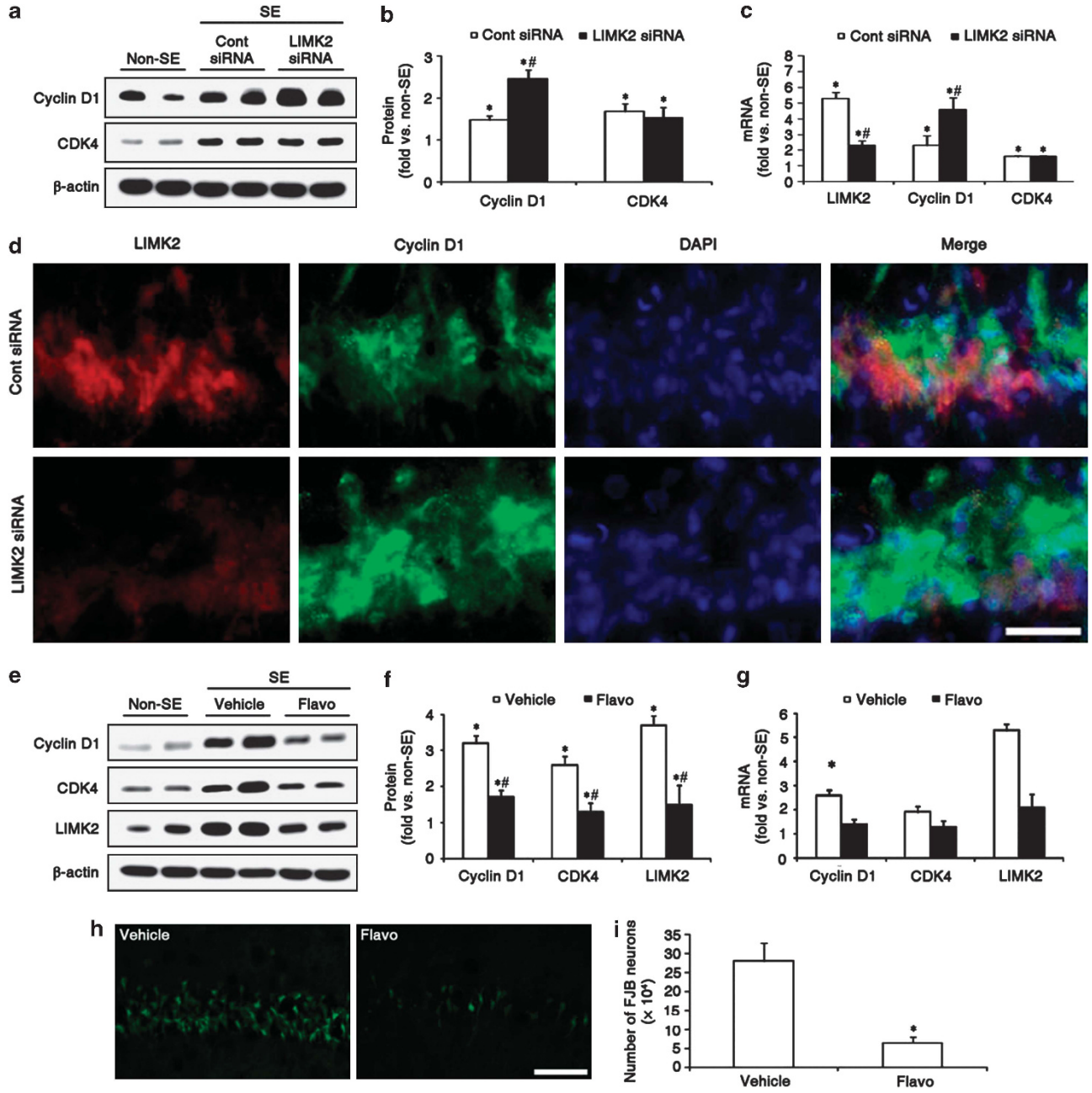

Figure 2 Reciprocal regulation of LIMK1 and cyclin D1/CDK4 complex following SE. (**a**–**d**) *LIMK2* siRNA elevates cyclin D1 mRNA/protein expression levels induced by SE. *LIMK2* siRNA cannot affect CDK4 mRNA/protein expression levels induced by SE. $^{*}P<0.05$ *versus* non-SE animals. $^{\#}P<0.05$ *versus* control siRNA-infused animals ($n=5$, respectively). Bar = 12.5 μm. (**e**–**g**) Flavopiridol (a cyclin D1/CDK4 inhibitor) significantly reduces cyclin D1, CDK4 and LIMK2 mRNA/protein expression levels. $^{*}P<0.05$ *versus* non-SE animals. $^{\#}P<0.05$ *versus* vehicle-treated animals ($n=5$, respectively). (**h** and **i**) Flavopiridol attenuates the number of FJB-positive neurons induced by SE. Bar = 50 μm. $^{*}P<0.05$ *versus* vehicle

cyclin D1, CDK4 and LIMK2 expression levels ($P<0.05$ *versus* vehicle, Figures 4a, c and d). Y-27632 also decreased LIMK2 T505 (not S283 or S291 + 293) and cofilin phosphorylation ($P<0.05$ *versus* vehicle, Figures 4a, c and d). Furthermore, Y-27632 alleviated SE-induced neuronal death ($P<0.05$ *versus* vehicle, Figures 4e and f). These findings indicate that ROCK activation may involve SE-induced neuronal death by reduction in $p27^{Kip1}$ expression.

LIMK2-mediated neuronal death is receptor interacting protein kinase 1 (RIP1)-independent programmed necrosis. Apoptosis and necrosis are two major cell death patterns.[27] Apoptosis is a highly regulated process involving the caspase family of cysteine proteases.[28] In contrast, necrosis is a passive and unregulated form of cell death. Some necrosis can be mediated by RIP1,[29,30] which is termed programmed necrosis or necroptosis.[31,32] Therefore,

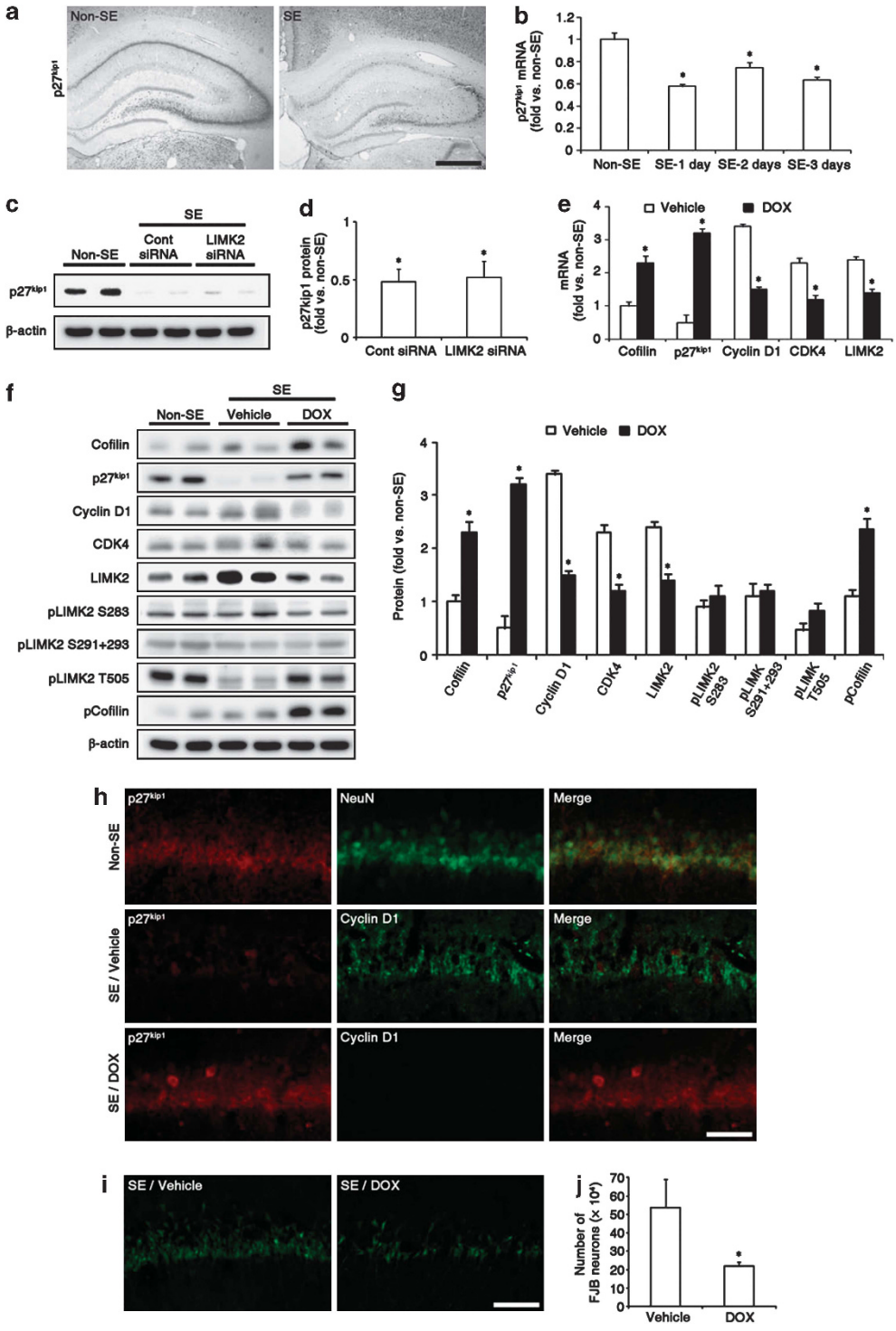

Figure 3 Role of $p27^{Kip1}$ in LIMK2-mediated neuronal death induced by SE. (**a**) SE decreases $p27^{Kip1}$ immunoreactivity in CA1 pyramidal cells that are vulnerable to SE insults. Bar = 400 μm. (**b** and **c**) $p27^{Kip1}$ mRNA/protein expression are reduced by SE. *$P<0.05$ *versus* non-SE animals ($n=5$, respectively). (**d**) *LIMK2* siRNA does not affect $p27^{Kip1}$ protein levels following SE. *$P<0.05$ *versus* non-SE animals ($n=5$, respectively). (**e–g**) DOX significantly increases cofilin and $p27^{Kip1}$ mRNA/protein expression levels and LIMK2 T505 and cofilin phosphorylations ($P<0.05$ *versus* vehicle), whereas it reduces cyclin D1, CDK4 and LIMK2 mRNA/protein expression levels induced by SE. *$P<0.05$ *versus* vehicle ($n=5$, respectively). (**h**) DOX effectively prevents the SE-induced reduction in $p27^{Kip1}$ expression accompanied by reduced cyclin D1 expression. Bar = 50 μm. (**i** and **j**) DOX effectively attenuates the number of FJB-positive neurons induced by SE. Bar = 50 μm. *$P<0.05$ *versus* vehicle ($n=5$, respectively)

we further investigated the relationship of LIMK2 over-expression with caspase-mediated apoptosis or RIP1-mediated necroptosis during neuronal death.

In the present study, SE did not affect the expression of Rb, pRb and active caspase-3 but increased E2F1 expression ($P<0.05$ *versus* non-SE animals, Figures 5a and b). *LIMK2*

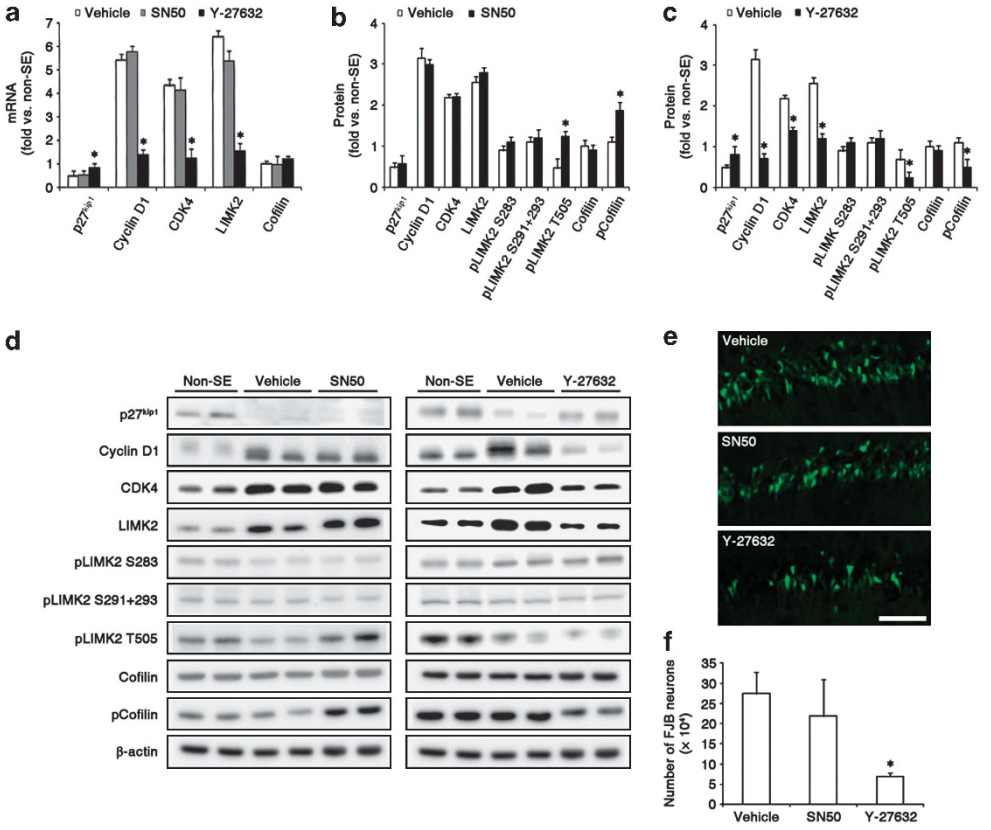

Figure 4 Role of ROCK and NFκB in LIMK2-mediated neuronal death induced by SE. (**a**–**d**) Y-27632 (a ROCK inhibitor), not SN50 (a NF-κB inhibitor), increases $p27^{Kip1}$ mRNA/protein expression following SE. Y-27632, not SN50, reduces cyclin D1, CDK4 and LIMK2 expression levels. Y-27632 also decreases LIMK2 T505 (not S283 or S291 + 293) and cofilin phosphorylations. *$P<0.05$ *versus* vehicle ($n=5$, respectively). (**e** and **f**) Y-27632, not SN50, attenuates the number of FJB-positive neurons induced by SE. Bar = 50 μm. *$P<0.05$ *versus* vehicle ($n=5$, respectively)

siRNA, DOX, flavopiridol and Y-27632 inhibited SE-induced E2F1 induction but increased Rb expression without alteration in Rb phosphorylation ($P<0.05$ *versus* vehicle or control siRNA, Figures 5a and b). These findings indicate that LIMK2-mediated neuronal death may not be relevant to apoptosis.

To confirm the role of LIMK2 in RIP1-mediated necroptosis, we investigated RIP1 expression following SE. SE did not affect RIP1 expression. *LIMK2* siRNA, DOX, flavopiridol and Y-27632 did not affect RIP1 expression following SE (Figures 5a and b). Necrostatin-1 (NEC-1, a RIP1 inhibitor) did not affect changes in LIMK2, Rb, pRb, active caspase-3 and RIP1 levels but inhibited E2F1 induction following SE ($P<0.05$ *versus* vehicle, Figures 5a and b). NEC-1 did not attenuate SE-induced neuronal death ($P<0.05$ *versus* vehicle, Figures 5c and d). These findings indicate that LIMK2-mediated neuronal death may not be RIP1-mediated necroptopsis. Together with translocation of HMGB1 to cytoplasm, swollen dendrites with disassembled microtubules and pyknotic nuclei, our findings indicate that LIMK2-mediated neuronal death may be RIP1-independent programmed necrosis.

LIMK2-mediated dynamic-related protein-1 (DRP1) inhibition induces neuronal death by dysfunction of mitochondrial fission. The remaining issue was the involvement of the effectors in LIMK2-mediated programmed necrotic neuronal death. Recently, hyperstabilization of actin filaments inhibits association of the fission protein DRP1 with mitochondria, leading to mitochondrial elongation and subsequent neurotoxicity.[33] In contrast to neurons, the induction of necroptosis in HT-29 and HeLa cells activates DRP1 by dephosphorylating the S637 site.[34] DRP1 is a soluble cytosolic protein that assembles into spiral filaments around mitochondrial tubules. DRP1 phosphorylation at S637 by protein kinase A inhibits fission by enhancing the dissociation of DRP1 from mitochondria. DRP1 phosphorylation at S616 activates mitochondrial fission by cyclin B–CDK1–RALA binding protein 1 (RALBP1) complex.[35] Thus, we investigated whether LIMK2-mediated neuronal death is relevant to dysfunction of mitochondrial fission.

In the present study, SE decreased DRP1 expression and DRP1 S616/S637 phosphorylation ratio, although it elevated RALBP1 expression ($P<0.05$ *versus* non-SE animals, Figures 6a–d). *LIMK2* siRNA, DOX, flavopiridol and Y-27632 treatment effectively prevented these alterations induced by SE ($P<0.05$ *versus* vehicle or control siRNA, Figures 6a–d). Furthermore, SE increased mitochondrial length and sphere formation in CA1 neurons ($P<0.05$ *versus* non-SE animals, Figures 7a and b). *LIMK2* siRNA, DOX, flavopiridol and Y-27632 treatment effectively prevented mitochondrial elongation and sphere formation induced by SE ($P<0.05$ *versus* vehicle or control siRNA, Figures 7a and b).

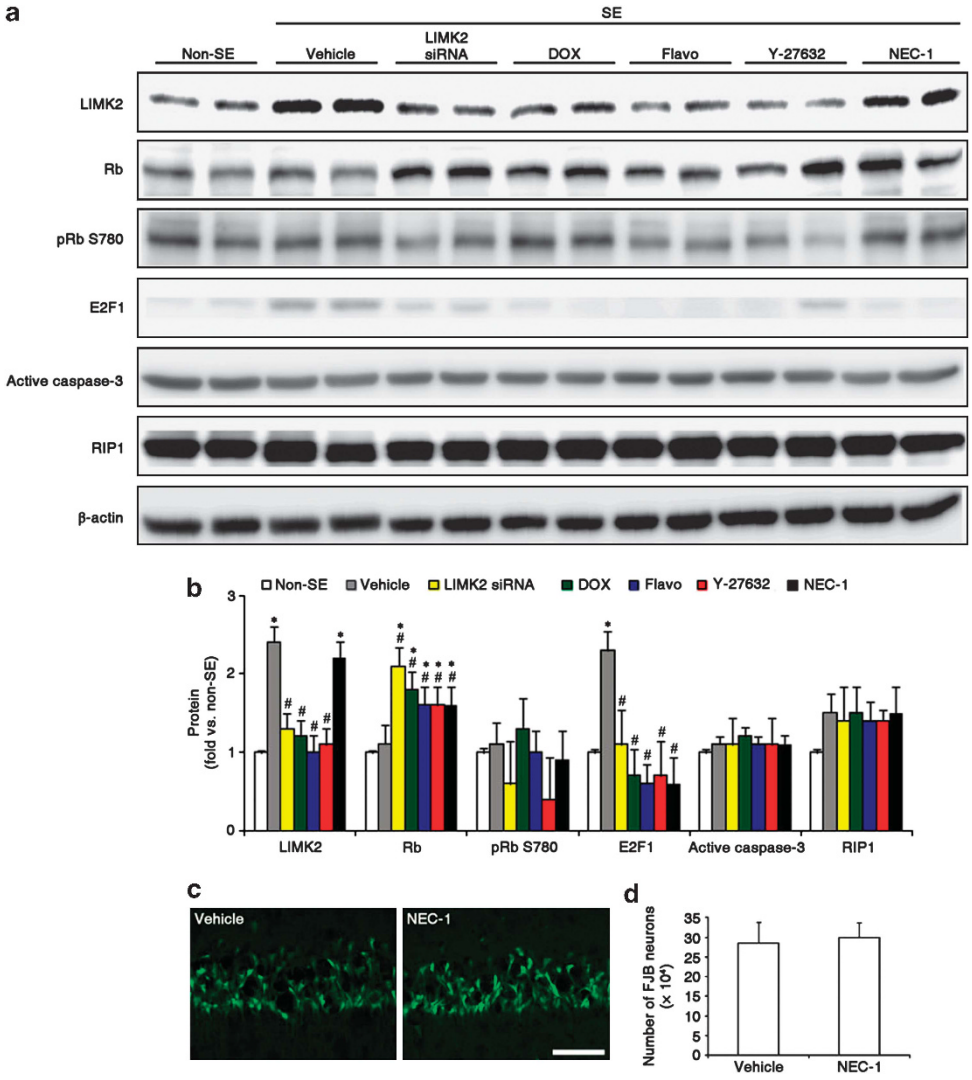

Figure 5 LIMK2-mediated neuronal death via caspase-3 or RIP1-independent pathway. (**a** and **b**) SE increases E2F1 expression, although it does not affect Rb, pRb and active caspase-3 expression levels. *LIMK2* siRNA, DOX, flavopiridol and Y-27632 increase Rb expression, while *LIMK2* siRNA, flavopiridol and Y-27632 infusion do not affect Rb S780 phosphorylation. Furthermore, *LIMK2* siRNA, DOX, flavopiridol and Y-27632 decrease E2F1 expression that is increased by SE and do not affect active caspase-3 expression following SE. SE does not affect RIP1 expression. *LIMK2* siRNA, DOX, flavopiridol and Y-27632 do not affect RIP1 expression induced by SE. NEC-1 (a RIP1 inhibitor) does not change LIMK2, Rb, pRb, active caspase-3 and RIP1 expression following SE, while it reduces E2F1 expression. $^{*}P<0.05$ *versus* non-SE animals. #$P<0.05$ *versus* vehicle or control siRNA ($n=5$, respectively). (**c** and **d**) NEC-1 does not affect SE-induced neuronal death ($n=5$, respectively). Bar = 50 μm

To address the issue of whether a decline of mitochondrial fission promotes neuronal cell death in response to SE, we applied Mdivi-1 (a DRP1 inhibitor) and WY 14643 (an enhancer of mitochondrial fission events) before SE.[36,37] As compared with vehicle, Mdivi-1 (5 and 50 μM) increased SE-induced mitochondrial elongation and neuronal death. The lowest dose of Mdivi-1 (0.5 μM) did not affect them (Figures 7c and d). Mdivi-1 (50 μM) did not affect LIMK2 overexpression induced by SE (Figure 7a). These findings indicate that Mdivi-1 may deteriorate LIMK2-mediated dysfunction of mitochondrial mission due to further reduction in DRP1 activity. In contrast to Mdivi-1, WY 14643 (150 μM) reduced mitochondrial length in non-SE animals as compared with vehicle ($P>0.05$ *versus* vehicle; Figures 8a and b). The lower doses (50 and 100 μM) of WY 14643 did not affect mitochondrial length in non-SE animals (data not shown). In addition, WY 14643 increased DRP1 S616 phosphorylation and DRP1 S616/S637 phosphorylation ratio without alterations in DRP1 expression and its S637 phosphorylation ($P<0.05$ *versus* vehicle; Figures 8c–e). WY 14643 effectively prevented mitochondrial elongation and sphere formation induced by SE ($P<0.05$ *versus* vehicle; Figures 8a and b). WY 14643 attenuated neuronal damage accompanied by reductions in DRP1 expression and S616 phosphorylation induced by SE ($P<0.05$ *versus* vehicle; Figures 8c–g). WY 14643 also inhibited the translocation of HMGB1 to cytoplasm induced by SE (Supplementary Figures S3a–c). These findings indicate that LIMK2-DRP1-mediated dysfunction of mitochondrial fragmentation may have an important role in the programmed necrotic cell death.

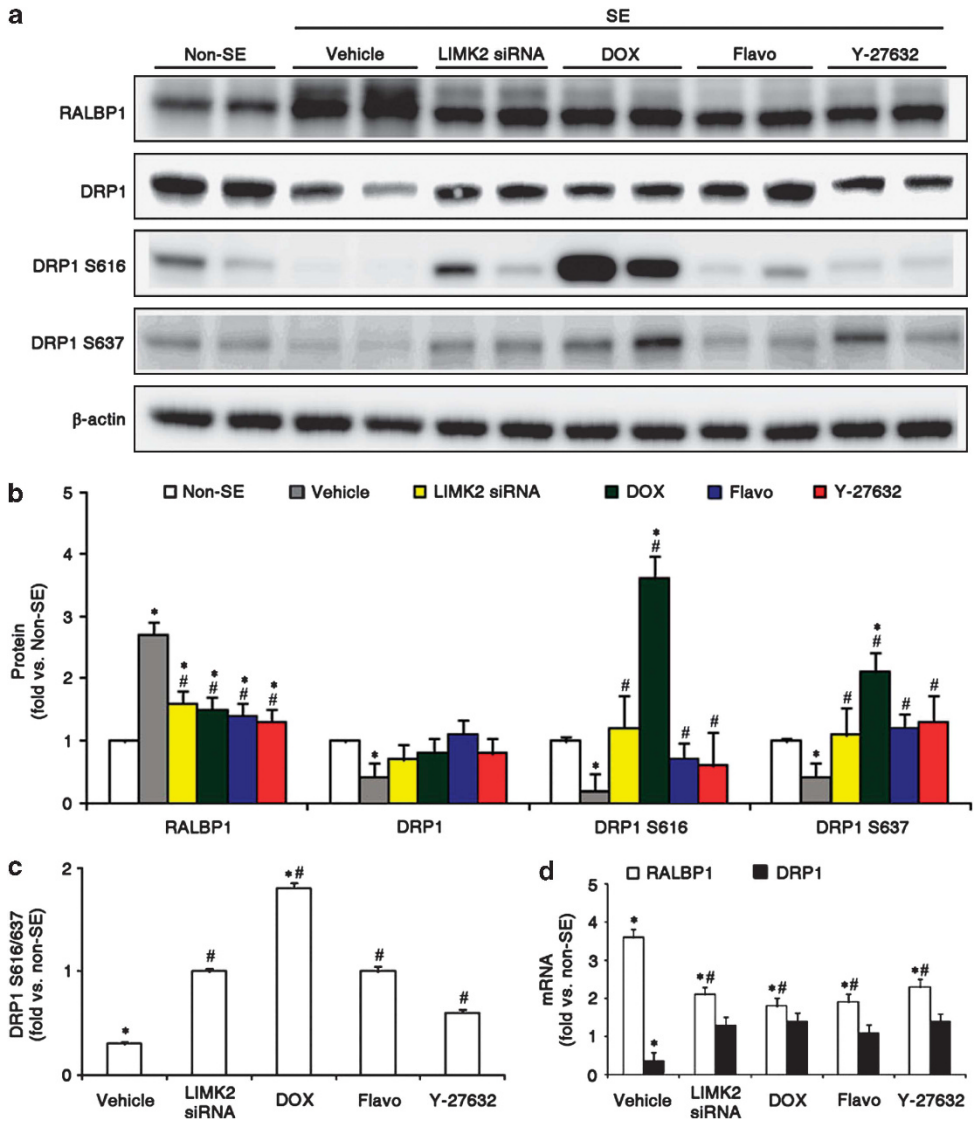

Figure 6 LIMK2-mediated downregulation of DRP1 expression following SE. (**a**–**d**) SE significantly elevates RALBP1 but decreases DRP1 expression and DRP1 S616/S637 phosphorylation. *LIMK2* siRNA, DOX, flavopiridol and Y-27632 effectively prevent these alterations induced by SE. *$P<0.05$ *versus* non-SE animals. #$P<0.05$ *versus* vehicle or control siRNA ($n=5$, respectively)

Discussion

Here, we describe a previously unsuspected role of LIMK2 in dysfunction of DRP1-mediated mitochondrial dynamics inducing programmed necrotic neuronal death. LIMK2 is one of the modulators of actin polymerization by cofilin phosphorylation. LIMK2 also has a role in actin-unrelated events, such as repression of cyclin D1.[17] In the present study, SE increased LIMK2 expression in dying neurons as a negative feedback response to inhibit SE-induced cyclin D1 expression. Furthermore, *LIMK2* siRNA attenuated necrotic neuronal damage induced by SE. These findings indicate that LIMK2 may be one of the essential molecules for cyclin D1/CDK4-mediated neuronal death.

Regulatory signaling pathway of cyclin D1/CDK4 complex in post-mitotic neurons remains unclear. Regardless of the underlying mechanism, neuroprotective effects of ROCK inhibitors from various neuronal injuries have been reported.[38,39] In the present study, ROCK inhibitor downregulated cyclin D1, CDK4 and LIMK2 expression induced by SE via enhanced $p27^{Kip1}$ expression. Furthermore, elevated $p27^{Kip1}$ expression by DOX prevented SE-induced neuronal death. These findings demonstrate for the first time the underlying mechanism for ROCK-mediated neuronal death through abnormal cell cycle re-entry by $p27^{Kip1}$ suppression. On the other hand, the effect of cofilin phosphorylation on induction of $p27^{Kip1}$ expression is unknown, although increased cofilin expression induces $p27^{Kip1}$ gene promotor transactivation.[21,22] In the present study, DOX increased cofilin phosphorylation/expression accompanied by increased $p27^{Kip1}$ expression. However, SN50 increased cofilin phosphorylation but did not alter cofilin and $p27^{Kip1}$ expression levels. These findings reveal that cofilin expression, not phosphorylation, may affect its efficiency for $p27^{Kip1}$ gene

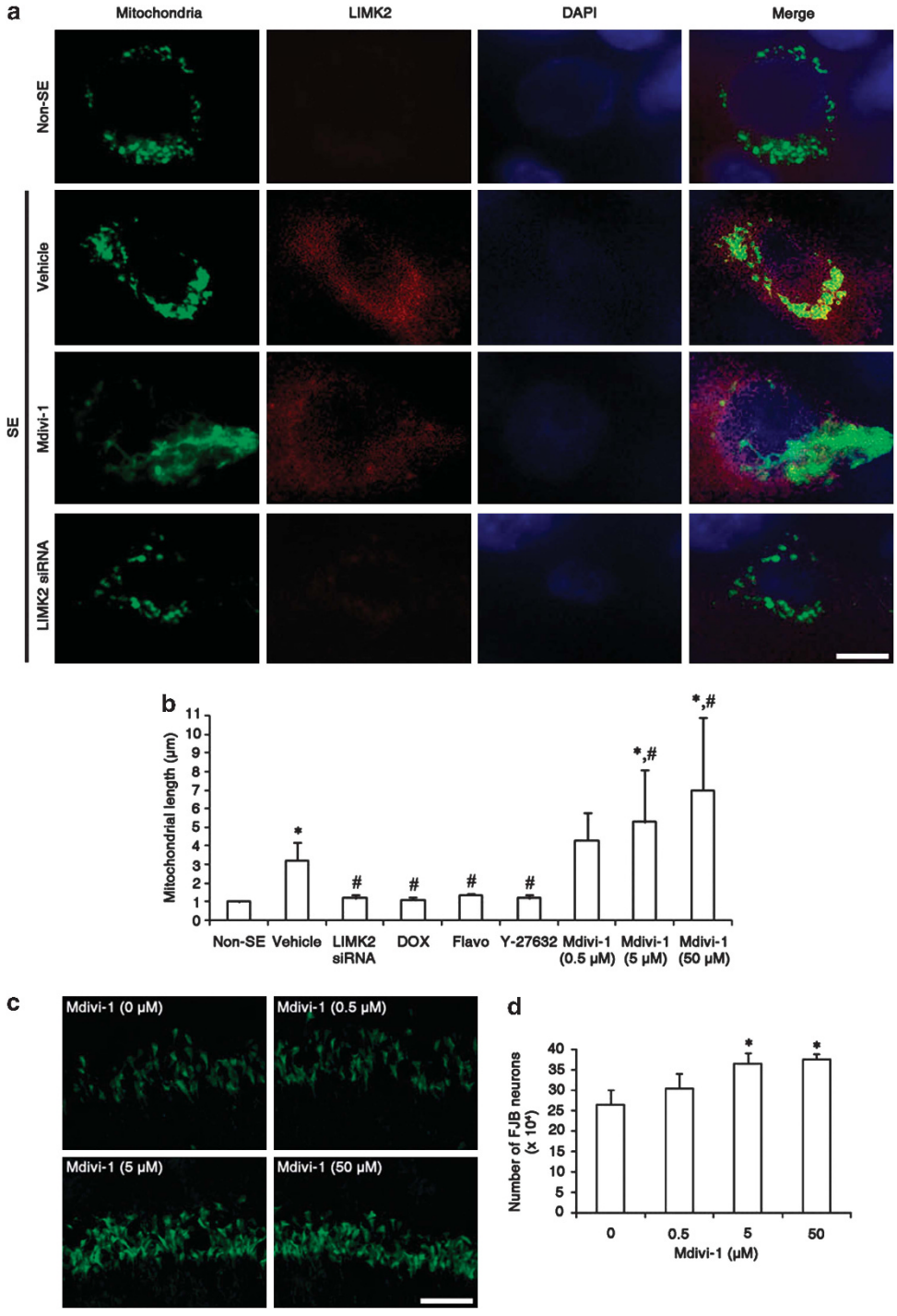

Figure 7 LIMK2-mediated dysfunction of mitochondrial fission induced by SE. (**a** and **b**) SE significantly increases mitochondrial length and sphere formation. Mdivi-1 (5 and 50 μM) effectively increases SE-induced mitochondrial length. *LIMK2* siRNA prevents elongation of mitochondrial length induced by SE. Bar = 6.25 μm. $^{*}P<0.05$ *versus* non-SE animals. $^{\#}P<0.05$ *versus* vehicle or control siRNA ($n=5$, respectively). (**c** and **d**) Mdivi-1 (5 and 50 μM) significantly increases the number of dying neurons following SE. Bar = 100 μm. $^{*}P<0.05$ *versus* vehicle ($n=5$, respectively)

promoter transactivation. Therefore, our findings suggest that the restoration of $p27^{Kip1}$ expression by regulation of ROCK activity or cofilin expression may be a new therapeutic strategy for cyclin D1/CDK4-mediated neurodegeneration.

Prevention of complications like hypoxia, hypotension, hypoglycemia and hyperpyrexia in SE do not inhibit neuronal death.[40,41] This SE-induced neuronal death is morphologically necrotic rather than apoptotic.[9–12] However, degenerating neurons also show apoptotic events.[42] Thus, it is debatable whether necrosis or apoptosis is the main process of neuronal death induced by seizure activity. In the present study, SE increased LIMK2 and translocation of HMGB1 from

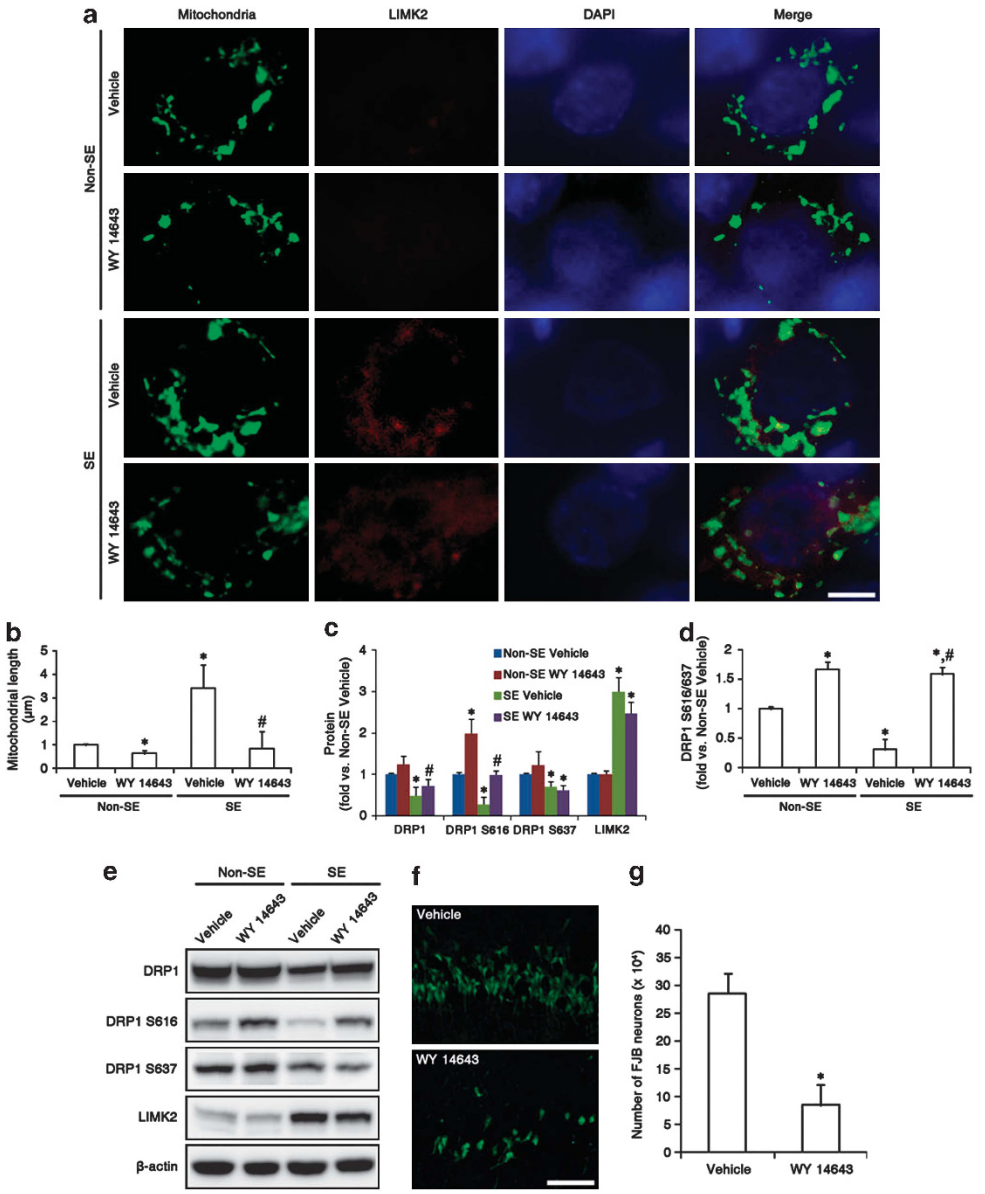

Figure 8 Effect of WY 14643 (150 μM) on mitochondrial fission and neuronal death following SE. (**a** and **b**) WY 14643 treatment effectively prevents elongation of mitochondrial length induced by SE. Bar = 6.25 μm. $^{*}P<0.05$ *versus* vehicle-treated animals in the non-SE group. $^{\#}P<0.05$ *versus* vehicle-treated animals in the SE group ($n=5$, respectively). (**c**–**e**) WY 14643 prevents alterations in DRP1 expression and DRP1 S616/S637 phosphorylation but not in LIMK2 expression, induced by SE. $^{*}P<0.05$ *versus* vehicle-treated animals in the non-SE group. $^{\#}P<0.05$ *versus* vehicle-treated animals in the SE group ($n=5$, respectively). (**f** and **g**) WY 14643 alleviated the number of dying neurons following SE. Bar = 100 μm. $^{*}P<0.05$ *versus* vehicle ($n=5$, respectively)

nucleus to cytoplasm but did not affect the expression of Rb, pRb, active caspase-3 or RIP1. *LIMK2* siRNA attenuated SE-induced necrotic degeneration characterized by translocation of HMGB1 to cytoplasm, swollen dendrites with disassembled microtubules and pyknotic nuclei. Taken together, our findings indicate that LIMK2 may participate in RIP1-independent programmed necrotic cell death but not in cyclin D1-Rb-E2F-caspase-dependent apoptosis.

The most interesting findings in the present study were that LIMK2 regulated mitochondrial swelling and mitochondrial fission by downregulation of DRP1 expression and DRP1 S616/S637 phosphorylation ratio independently of actin polymerization during programmed necrosis. Recently, hyperstabilization of F-actin by tau was reported as being critical for neurotoxicity due to inhibition of DRP1.[33] Therefore, it is presumable that LIMK2 overexpression would inhibit mitochondrial fission by increasing actin stabilization. In the present study, however, SE decreased F-actin content, DRP1 expression and DRP1 S616/S637 phosphorylation ratio, whereas it increased mitochondrial length and sphere formation. *LIMK2* siRNA, flavopiridol, Y-27632 and DOX prevented these pathological changes induced by SE. Furthermore, WY 14643 significantly attenuated mitochondrial elongation and neuronal death induced by SE, whereas Mdivi-1 increased them. A loss of mitochondrial fission results in improper segregation of mitochondria and a decrease in ATP

levels.[33] Elongated mitochondria induced by inhibiting DRP1 are not properly localized to either dendrites or axons and suppresses ATP supply in peripheral sites.[41,42] DRP1 deletion also results in impairment of respiratory function in mitochondria due to oxidative stress that can lead to further increases in the production of reactive oxygen species.[43,44] In cultured postnatal mouse cortical neurons, DRP1 overexpression enhances neuronal viability and restores a normal pattern of mitochondrial morphology following DNA damage.[45] Furthermore, DRP1 is required for a normal rate of cytochrome *c* release and caspase activation during apoptosis.[46] Therefore, our findings indicate that LIMK2 overexpression may lead to neuronal death by dysfunction of DRP1-mediated mitochondrial fission and that downregulation of DRP1 expression may accelerate necrosis rather than apoptosis.

In the present study, we cannot directly address the mechanism by which LIMK2 suppresses DRP1 expression level. However, it is presumable that LIMK2 would regulate DRP1 expression via cell-cycle related events, which is unknown at present. Horn *et al.*[47] reported that DRP1 level drops when cells enter G1 phase, and in turn, DRP1 level gradually increases following release from G1/S arrest. As cyclin D1 is required for G1/S transition and LIMK2 suppresses cyclin D1 expression,[17] overexpression of cyclin D1 followed by LIMK2 could lead neurons to G1/S arrest-like condition that sustains decrease in DRP1 level. Further studies are needed to elucidate the exact mechanism of LIMK2-mediated DRP1 supression.

RALBP1 is a key player to phosphorylate DRP1 S616, which is an effector of mitochondrial fragmentation.[33] In the present study, SE increased RALBP1 expression, although it reduced mitochondrial fission. Furthermore, *LIMK2* siRNA, flavopiridol, Y-27632 and DOX effectively prevented necrotic neuronal death and upregulation of RALBP1 expression induced by SE. These findings indicate that RALBP1 may not be relevant to DRP1-related neuronal death. RALBP1 is a stress-responsive, multi-functional protein with multi-specific transport activity.[48] RALBP1 accounts for up to 80% of the transport of glutathione-conjugates.[48] Furthermore, blockade of RALBP1 function cells results in the accumulation of 4-hydroxynonenal (a product of lipid peroxidation) and its GSH-conjugate that occur a massive apoptosis.[14,49] Therefore, upregulated RALBP1 may be one of the common compensatory phenomena in responses to oxidative stress rather than mitochondrial fission.

In summary, we provide novel evidence that ROCK-$p27^{Kip1}$-Cyclin D1-CDK4-LIMK2-DRP1-mediated signal is associated with neuronal necrosis, not apoptosis, by microchondrial dysfunction (Supplementary Figure S4). To the best of our knowledge, the present study proposes for the first time the role of RIP-independent programmed necrosis in neuronal degeneration. Beyond new insights in neuronal death, this regulatory pathway will be an interesting and important therapeutic target for various diseases relating to programmed necrosis or aberrant cell cycle.

Materials and Methods

Experimental animals and chemicals. This study utilized male Sprague-Dawley rats (7 weeks old) obtained from Experimental Animal Center, Hallym University, Chunchon, Republic of Korea. The animals were provided with a commercial diet and water *ad libitum* under controlled temperature, humidity and lighting conditions ($22 \pm 2\,^{\circ}C$, $55 \pm 5\%$ and a 12 : 12 light/dark cycle). Animal protocols were approved by the Institutional Animal Care and Use Committee of Hallym University (Chunchon, Republic of Korea). The number of animals used and their suffering was minimized in all cases. All reagents were obtained from Sigma-Aldrich (St. Louis, MO, USA), except as noted.

Surgery, drug infusion and LIMK2 knockdown. Animals were divided into six groups for intracerebroventricular drug infusion: (1) vehicle, (2) Flavo (50 μM) (3) Y-27632 (10 μM), (4) NEC-1 (900 μM), (5) Mdivi-1(0.5, 5 and 50 μM), or (6) WY 14643 (50, 100 and 150 μM), and one group for intraperitoneal injection of DOX (50 mg/kg). Animals were anesthetized (Zolretil, 50 mg/kg, I.M. Virbac Laboratories, Carros, France) and placed in a stereotaxic frame. For the osmotic pump implantation, holes were drilled through the skull for introducing a brain infusion kit 1 (Alzet, Cupertino, CA, USA) into the right lateral ventricle (1 mm posterior; 1.5 mm lateral; -3.5 mm depth), according to the atlas.[50] The infusion kit was sealed with dental cement and connected to an osmotic pump (1007D, Alzet). The pump was placed in a subcutaneous pocket in the dorsal region. Animals received 0.5 μl/h of vehicle or compound over 1 week.[51] For knockdown of LIMK2, we applied a set of four on-target *LIMK2* rat siRNAs and a nontargeting control were used. Of the four, a 21-nt siRNA sequence targeting *LIMK2* corresponding to coding region ($5' \rightarrow 3'$): sense: GCACCUUACGCAAGAGUGAUU, and antisense: UCACUCUUGCGUAAGGUGCUU was selected as the best probe (reduction efficiency, 79.41% in control condition) and used for the final experiments. A nonsilencing RNA was used as the control siRNA. siRNA was infused over 2 weeks using 1002 osmotic mini-pumps (0.35 mg/day siRNA in saline, ALZET Osmotic Pumps, Cupertino, CA, USA). The dosage of the drugs and siRNA were chosen based on preliminary studies indicating that administration of up to the chosen dose was well tolerated, and no signs of neurotoxicity (hind-limb paralysis, vocalization, food intake or neuroanatomical damage) were observed. The dosage of each compound and siRNA was determined as the highest dose that did not affect seizure threshold in the preliminary study. The compounds or siRNA began to be immediately infused after surgery. Rats were allowed 3 days to recover from the surgical procedure before SE induction.

SE induction. Three days after surgery, rats were treated with pilocarpine (380 mg/kg, i.p.) 20 min after methylscopolamine (5 mg/kg, i.p.). Diazepam (10 mg/kg, i.p.) was administered 2 h after the onset of SE and repeated as needed.

Tissue processing. At designated time points, the animals were perfused transcardially with phosphate-buffered saline (PBS) followed by 4% paraformaldehyde in 0.1 M phosphate buffer (pH 7.4) under urethane anesthesia (1.5 g/kg, i.p.). The brains were removed and postfixed in the same fixative for 4 h. The brains were infiltrated with 30% sucrose overnight, frozen and sectioned with a cryostat at 30 μm, and consecutive sections were stored in six-well plates containing PBS. Every sixth section in the series throughout the entire hippocampus was used for stereological study.[52]

Immunohistochemistry. Table 1 provides a list of the primary antibodies used. Sections were incubated in a mixture of antisera in PBS containing 0.3% Triton X-100 overnight at room temperature. After washing three times for 10 min with PBS, the sections were also incubated in a mixture of FITC- and Cy3-conjugated secondary antisera (or streptavidin, 1 : 250, Amersham, Piscataway, NJ, USA) for 2 h at room temperature. Some sections were used for conventional immunohistochemical study. The sections were washed three times for 10 min with PBS and mounted on gelatin-coated slides. All images were captured using an Axio Imager M2 microscope and AxioVision Rel. 4.8 software (Carl Zeiss Korea, Seoul, Republic of Korea). For quantitative analysis of fluorescent intensity, sections (15 sections per one animal) were viewed through a microscope connected via CCD camera (Carl Zeiss Korea) to a PC monitor (SAMSUNG, Seoul, Republic of Korea). Each image was normalized by adjusting the black and white range of the image using Adobe PhotoShop v. 8.0 (San Jose, CA, USA). Thereafter, intensity measurements were represented as the number of a 256-gray scale using the NIH Image 1.59 software (http://rsb.info.nih.gov/nih-image/download.html). Optical density values were corrected by subtracting the average values of background noise obtained from five image inputs. The optical density was then standardized by setting the threshold levels.

Table 1 Primary antibodies used in the present study

Antigen	Host	Manufacturer (catalog number)	Dilution used
Active caspase-3	Rabbit	Abcam (ab13847, Cambridge, MA, USA)	IF 1 : 200, WB 1 : 1000
CDK4	Mouse	Abbiotec (251727, San Diego, CA, USA)	IF 1 : 200, WB 1 : 500
Cofilin	Rabbit	Sigma (C8736, St. Louis, MO, USA)	WB 1 : 20k
Cyclin D1	Mouse	Abcam (ab6152)	IF 1 : 2000, WB 1 : 1000
DRP1	Rabbit	Thermo (PA1-16987, Hudson, NH, USA)	WB 1 : 1000
E2F1	Mouse	Abcam (ab4070)	WB 1 : 1000
LIMK1	Rabbit	Abcam (ab81046)	WB 1 : 1000
LIMK2	Rabbit	Sigma (HPA008183)	IF 1 : 100, WB 1 : 1000
Mitochondrial marker	Mouse	Abcam (ab14705)	IF 1 : 500
$p27^{Kip1}$	Rabbit	Abcam (ab7961)	IF 1 : 100, WB 1 : 500
pCofilin	Rabbit	Abcam (ab47281)	WB 1 : 2000
pDRP1 S616	Rabbit	Cell Signaling (4494, Danvers, MA, USA)	WB 1 : 1000
pDRP1 S637	Rabbit	Cell Signaling (4867)	WB 1 : 1000
pLIMK2 S283	Rabbit	Assay Biotech (A8045, Sunnyvale, CA, USA)	IF 1 : 100, WB 1 : 1000
pLIMK2 S291 + 293	Rabbit	Abcam (ab76284)	IF 1 : 100, WB 1 : 500
pLIMK2 T505	Rabbit	Abcam (ab38499)	IF 1 : 100, WB 1 : 1000
pRb S780	Rabbit	Abcam (ab47763)	IF 1 : 100, WB 1 : 1000
RALBP1	Rabbit	Abcam (ab133549)	IF 1 : 200, WB 1 : 5000
Rb	Rabbit	Abcam (ab85607)	IF 1 : 200, WB 1 : 1000
RIP	Rabbit	Abcam (ab106393)	WB 1 : 1000
β-Actin	Mouse	Sigma (A5316)	WB 1 : 5000
HMGB1	Rabbit	Abcam (ab18256)	IF 1 : 100

Abbreviations: IF, immunofluorescence; WB, western blotting

TUNEL staining. TUNEL staining was performed with the TUNEL apoptosis detection kit (Upstate, Lake Placid, NY, USA) according to the manufacturer's protocol (http://www.upstate.com). Following the TUNEL reaction, LIMK2 or cyclin D1 immunofluorescence staining was performed. For nuclei counterstaining, we used Vectashield mounting medium with DAPI (Vector, Burlingame, CA, USA). All images were captured using an Axiocam HRc camera and Axio Vision 3.1 software (Carl Zeiss Korea).

FJB staining. FJB staining was used to identify degenerating neurons. Briefly, sections were rinsed in distilled water and mounted onto gelatin-coated slides and then dried on a slide warmer. The slides were immersed in 100% ethanol for 3 min, followed by 70% ethanol for 2 min and distilled water for 2 min. The slides were then transferred to 0.06% potassium permanganate for 15 min and gently agitated. After rinsing in distilled water for 2 min, the slides were incubated for 30 min in 0.001% FJB (Histo-Chem Inc. Jefferson, AR, USA), freshly prepared by adding 20 ml of a 0.01% stock FJB solution to 180 ml of 0.1% acetic acid, with gentle shaking in the dark. After rinsing for 1 min in each of three changes of distilled water, the slides were dried, dehydrated in xylene and coverslipped with DPX. For stereological study, every sixth section in the series throughout the entire hippocampus was used (see below).

Stereology. The hippocampal volumes (V) were estimated according to the formula based on the modified Cavalieri method: $V = \Sigma a \times t_{nom} \times 1/ssf$, where a is area of the region of the delineated subfield measured by AxioVision Rel. 4.8 software, t_{nom} is the nominal section thickness (of 30 μm in this study) and ssf is the fraction of the sections sampled or section sampling fraction (of 1/6 in this study). The volumes are reported as mm^3. The subfield areas were delineated with a 2.5 $\times$ objective lens.[52] The optical fractionator was used to estimate the cell numbers. The optical fractionator (combination of performing counting with the optical disector, with fractionator sampling) is a stereological method based on a properly designed systematic random sampling method that by definition yields unbiased estimates of population number. The sampling procedure is accomplished by focusing through the depth of the tissue (the optical disector height, h; of 15 μm in all cases for this study). The number of each cell type (C) in each of the subregions is estimated as: $C = \Sigma Q^- \times t/h \times 1/asf \times 1/ssf$, where Q^- is the number of cells actually counted in the disectors that fell within the sectional profiles of the subregion seen on the sampled sections, and asf is the areal sampling fraction calculated by the area of the counting frame of the dissector, a(frame) (of 50×50 μm^2 in this study) and the area associated with each x, y movement, grid (x, y step) (of 250×250 μm^2 in this study) (asf = (a(frame)/a(x,y step))). Cells were counted with a $\times$ 40objective lens. Individual mitochondrion length in CA1 pyramidal cells ($n = 20$/section) was also measured with a $\times$ 100objective lens by AxioVision Rel. 4.8 software. Cell counts and measurement of mitochondrion length were performed by two different investigators who were blind to the classification of tissues.[52]

Table 2 Coding sequences of each target gene used in the present study

Target gene	Sequences (5′→3′)
CDK4	Forward: GCCTGTGGTTGTTACGCTCT
	Reverse: CTGGTCAGCCTCAGAGTTCC
Cofilin	Forward: TTCTGGTAGGAGATGTGGGG
	Reverse: ACCAGGTCCTCCTTCTTGCT
Cyclin D1	Forward: GCACAACGCACTTTCTTTCC
	Reverse: TCCAGAAGGGCTTCAATCTG
DRP1	Forward: GGTGGAATTGGAGATGGTGGTCGA
	Reverse: TTCGTGCAACTGGAACTGGCACA
LIMK2	Forward: CTTCCTGTGTTGTCCGCGCC
	Reverse: AGGCCTCGTTGGCTGTCCTG
$p27^{Kip1}$	Forward: GGTGGACCAAATGCCTGACT
	Reverse: GCCCTTTTGTTTTGCGAAGA
RALBP1	Forward: AAGGTGTCCTCGAGGTGAGA
	Reverse: GGAGTCAGACGTGTGCAAGA
Caspase 3	Forward: CATGACCCGTCCCTT
	Reverse: CCGACTTCCTGTATGCTT
Drp-1	Forward: GGTGGAATTGGAGATGGTGGTCGA
	Reverse: TTCGTGCAACTGGAACTGGCACA
RIP	Forward: GCTCACCTCCCGTGAGTC
	Reverse: GGAGCTAGGTGCTGAAGTGG
GAPDH	Forward: TGGAGTCTACTGGCGTCTT
	Reverse: TGTCATATTTCTCGTGGTTCA

Western blotting. Tissue lysate proteins were loaded into a 10% polyacrylamide gel. After electrophoresis, gels were transferred to nitrocellulose transfer membranes (Schleicher and Schuell BioScience Inc., Keene, NH, USA). To reduce background staining, the filters were incubated with 5% nonfat dry milk in TBS containing 0.1% Tween 20 for 45 min, followed by incubation first with the primary antibody (Table 1) and subsequently with an HRP-conjugated secondary antibody. Western blotting was performed with an ECL Western Blotting Detection Kit (Amersham). Intensity measurements were represented as the mean gray-scale value on a 256 gray-level scale.[51]

RNA extraction, reverse transcription and quantitative real-time PCR. Brain tissues were homogenized and total RNA was extracted using Trizol Reagents, according to the manufacturer's protocol (Ambion, Austin, TX, USA). Total RNA was reverse transcribed into first-strand cDNA using a PrimerScript 1st strand cDNA synthesis kit (Takara, Shiga, Japan). Quantification of mRNA expression was performed in triplicate using a SYBR Green SuperMix (Bioneer, Taejon, South Korea) in a two-step PCR reaction procedure, performed with the MyiQ Single Color Real-Time PCR Detection System (Bioneer, Taejon, South Korea). Ten microliters of cDNA from the RT-reaction was used as the template for the quantitative real-time PCR reaction with a final PCR reaction volume of 50 μl. The 5′ and 3′ gene-specific PCR primer concentrations were 10 pM each. Real-time PCR primers were designed using the Primer3 software (Whitehead Institute, Cambridge, MA, USA) according to the coding sequences of each target gene (Table 2). After initial denaturation at 95 °C for 3 min, 40 cycles of primer annealing and elongation were performed at 60 °C for 45 s, followed by denaturation at 95 °C for 10 s. Fluorescence emission data were captured, and mRNA levels were quantified using the threshold cycle value (Ct). To compensate for variations in input RNA amounts and efficiency of reverse transcription, qPCR data for mRNA for each sample were normalized to the housekeeping protein GAPDH (GenBank no. BC063166) determined from the same experiment.

Data analysis. All data obtained from the quantitative measurements were analyzed using one-way ANOVA to determine statistical significance. Bonferroni's test was used for *post-hoc* comparisons. A *P*-value <0.05 was considered statistically significant.[51]

Conflict of Interest

The authors declare no conflict of interest.

Acknowledgements. This work was supported by the National Research Foundation of Korea (NRF) grant funded by the Korea government (MEST) (Nos. 2012R1A2A1A01001775 and 2009-0093812).

1. Stoica BA, Byrnes KR, Faden AI. Cell cycle activation and CNS injury. *Neurotox Res* 2009; **16**: 221–237.
2. Greene L, Biswas S, Liu D. Cell cycle molecules and vertebrate neuron death: E2F at the hub. *Cell Death Differ* 2004; **11**: 49–60.
3. Nguyen M, Boudreau M, Kriz J, Couillard-Despres S, Kaplan D, Julien J. Cell cycle regulators in the neuron death pathway of amyotrophic lateral sclerosis caused by mutant superoxide dismutase. *J Neurosci* 2003; **23**: 2131–2140.
4. Ino H, Chiba T. Cyclin-dependent kinase 4 and cyclin D1 are required for excitotoxin-induced neuronal cell death *in vivo*. *J Neurosci* 2001; **21**: 6086–6094.
5. Timsit S, Rivera S, Ouaghi P, Guischard F, Tremblay E, Ben-Ari Y *et al.* Increased cyclin D1 in vulnerable neurons in the hippocampus after ischaemia and epilepsy: a modulator of *in vivo* programmed cell death? *Eur J Neurosci* 1999; **11**: 263–278.
6. Park DS, Obeidat A, Giovanni A, Greene LA. Cell cycle regulators in neuronal death evoked by excitotoxic stress: implications for neurodegeneration and its treatment. *Neurobiol Aging* 2000; **21**: 771–781.
7. Li Y, Chopp M, Powers C, Jiang N. Immunoreactivity of cyclin D1/cdk4 in neurons and oligodendrocytes after focal cerebral ischemia in rat. *J Cereb Blood Flow Metab* 1997; **17**: 846–856.
8. Li Y, Jiang N, Powers C, Chopp M. Neuronal damage and plasticity identified by microtubule-associated protein 2, growth-associated protein 43, and cyclin D1 immunoreactivity after focal cerebral ischemia in rats. *Stroke* 1998; **29**: 1972–1981.
9. Ingvar M, Morgan PF, Auer RN. The nature and timing of excitotoxic neuronal necrosis in the cerebral cortex, hippocampus and thalamus due to flurothyl-induced status epilepticus. *Acta Neuropathol* 1988; **75**: 362–369.
10. Olney JW, Rhee V, Ho OL. Kainic acid: a powerful neurotoxic analogue of glutamate. *Brain Res* 1974; **77**: 507–512.
11. Schwob JE, Fuller T, Price JL, Olney JW. Widespread patterns of neuronal damage following systemic or intracerebral injections of kainic acid: a histological study. *Neuroscience* 1980; **5**: 991–1014.
12. Sloviter RS, Dean E, Sollas AL, Goodman JH. Apoptosis and necrosis induced in different hippocampal neuron populations by repetitive perforant path stimulation in the rat. *J Comp Neurol* 1996; **366**: 516–533.
13. Bamburg JR, McGough A, Ono S. Putting a new twist on actin: ADF/cofilins modulate actin dynamics. *Trends Cell Biol* 1999; **9**: 364–370.
14. Yang Y, Sharma R, Sharma A, Awasthi S, Awasthi YC. Cofilin phosphorylation by LIM-kinase 1 and its role in Rac-mediated actin reorganization. *Nature* 2003; **393**: 809–812.
15. Amano T, Tanabe K, Eto T, Narumiya S, Mizuno K. LIM-kinase 2 induces formation of stress fibers, focal adhesions and membrane blebs, dependent on its activation by Rho-associated kinase-catalysed phosphorylation at threonine-505. *Biochem J* 2001; **354**: 149–159.
16. Chua BT, Volbracht C, Tan KO, Li R, Yu VC, Li P. Mitochondrial translocation of cofilin is an early step in apoptosis induction. *Nat Cell Biol* 2003; **5**: 1083–1089.
17. Goyal P, Pandey D, Behring A, Siess W. Inhibition of nuclear import of LIMK2 in endothelial cells by protein kinase C-dependent phosphorylation at Ser-283. *J Biol Chem* 2005; **280**: 27569–27577.
18. Scaffidi P, Misteli T, Bianchi ME. Release of chromatin protein HMGB1 by necrotic cells triggers inflammation. *Nature* 2002; **418**: 191–195.
19. Faraco G, Fossati S, Bianchi ME, Patrone M, Pedrazzi M, Sparatore B *et al.* High mobility group box 1 protein is released by neural cells upon different stresses and worsens ischemic neurodegeneration *in vitro* and *in vivo*. *J Neurochem* 2007; **103**: 590–603.
20. Toyoshima H, Hunter T. p27, a novel inhibitor of G1 cyclin-Cdk protein kinase activity, is related to p21. *Cell* 1994; **78**: 67–74.
21. Lee YJ, Mazzatti DJ, Yun Z, Keng PC. Inhibition of invasiveness of human lung cancer cell line H1299 by over-expression of cofilin. *Cell Biol Int* 2005; **29**: 877–883.
22. Tsai CH, Chiu SJ, Liu CC, Sheu TJ, Hsieh CH, Keng PC *et al.* Regulated expression of cofilin and the consequent regulation of p27(Kip1) are essential for G(1) phase progression. *Cell Cycle* 2009; **8**: 2365–2374.
23. Liang ZQ, Wang X, Li LY, Wang Y, Chen RW, Chuang DM *et al.* Nuclear factor-kappaB-dependent cyclin D1 induction and DNA replication associated with N-methyl-D-aspartate receptor-mediated apoptosis in rat striatum. *J Neurosci Res* 2007; **85**: 1295–1309.
24. Prasad RC, Wang XL, Law BK, Davis B, Green G, Boone B *et al.* Identification of genes, including the gene encoding p27Kip1, regulated by serine 276 phosphorylation of the p65 subunit of NF-kappaB. *Cancer Lett* 2009; **275**: 139–149.
25. Ryu HJ, Kim JE, Yeo SI, Kim MJ, Jo SM, Kang TC. ReLA/P65-serine 536 nuclear factor-kappa B phosphorylation is related to vulnerability to status epilepticus in the rat hippocampus. *Neuroscience* 2011; **187**: 93–102.
26. Croft DR, Olson MF. The Rho GTPase effector ROCK regulates cyclin A, cyclin D1, and p27Kip1 levels by distinct mechanisms. *Mol Cell Biol* 2006; **26**: 4612–4627.
27. Kroemer G, Galluzzi L, Vandenabeele P, Abrams J, Alnemri ES, Baehrecke EH *et al.* Classification of cell death: recommendations of the Nomenclature Committee on Cell Death 2009. *Cell Death Differ* 2009; **16**: 3–11.
28. Earnshaw WC, Martins LC, Kaufmann SH. Mammalian caspases: structure, activation, substrates, and functions during apoptosis. *Annu Rev Biochem* 1999; **68**: 383–424.
29. Festjens N, Vanden Berghe T, Vandenabeele P. Necrosis, a well-orchestrated form of cell demise: signalling cascades, important mediators and concomitant immune response. *Biochim Biophys Acta* 2006; **1757**: 1371–1387.
30. Golstein P, Kroemer G. Cell death by necrosis: towards a molecular definition. *Trends Biochem Sci* 2007; **32**: 37–43.
31. Degterev A, Huang Z, Boyce M, Li Y, Jagtap P, Mizushima N *et al.* Chemical inhibitor of nonapoptotic cell death with therapeutic potential for ischemic brain injury. *Nat Chem Biol* 2005; **1**: 112–119.
32. Vandenabeele P, Declercq W, Van Herreweghe F, Vanden Berghe T. The role of the kinases RIP1 and RIP3 in TNF-induced necrosis. *Sci Signal* 2010; **3**: re4.
33. DuBoff B, Götz J, Feany MB. Tau promotes neurodegeneration via DRP1 mislocalization *in vivo*. *Neuron* 2012; **75**: 618–632.
34. Wang Z, Jiang H, Chen S, Du F, Wang X. The mitochondrial phosphatase PGAM5 functions at the convergence point of multiple necrotic death pathways. *Cell* 2012; **148**: 228–243.
35. Kashatus DF, Lim KH, Brady DC, Pershing NL, Cox AD, Counter CM. RALA and RALBP1 regulate mitochondrial fission at mitosis. *Nat Cell Biol* 2011; **13**: 1108–1115.
36. Lundgren B, Bergstrand A, Karlsson K, DePierre JW. Effects of dietary treatment with clofibrate, nafenopin or WY-14.643 on mitochondria and DNA in mouse liver. *Biochim Biophys Acta* 1990; **1035**: 132–138.
37. Zolezzi JM, Silva-Alvarez C, Ordenes D, Godoy JA, Carvajal FJ, Santos MJ *et al.* Peroxisome proliferator-activated receptor (PPAR) γ and PPARα agonists modulate mitochondrial fusion-fission dynamics: relevance to reactive oxygen species (ROS)-related neurodegenerative disorders? *PLoS One* 2013; **8**: e64019.
38. Rikitake Y, Kim HH, Huang Z, Seto M, Yano K, Asano T *et al.* Inhibition of Rho kinase (ROCK) leads to increased cerebral blood flow and stroke protection. *Stroke* 2005; **36**: 2251–2257.
39. Villar-Cheda B, Dominguez-Meijide A, Joglar B, Rodriguez-Perez AI, Guerra MJ, Labandeira-Garcia JL. Involvement of microglial RhoA/Rho-kinase pathway activation in the dopaminergic neuron death. Role of angiotensin via angiotensin type 1 receptors. *Neurobiol Dis* 2012; **47**: 268–279.
40. Meldrum BS, Brierley JB. Prolonged epileptic seizures in primates: ischemic cell change and its relation to ictal physiological events. *Arch Neurol* 1973; **28**: 10–17.
41. Meldrum BS, Vigouroux RA, Brierley JB. Systemic factors and epileptic brain damage: prolonged seizures in paralyzed, artificially ventilated baboons. *Arch Neurol* 1973; **29**: 82–87.
42. Sankar R, Shin DH, Liu H, Mazarati A, Pereira de Vasconcelos A, Wasterlain CG. Patterns of status epilepticus-induced neuronal injury during development and long-term consequences. *J Neurosci* 1998; **18**: 8382–8393.
43. Kageyama Y, Zhang Z, Roda R, Fukaya M, Wakabayashi J, Wakabayashi N *et al.* Mitochondrial division ensures the survival of postmitotic neurons by suppressing oxidative damage. *J Cell Biol* 2012; **197**: 535–551.

44. Parone PA, Da Cruz S, Tondera D, Mattenberger Y, James DI, Maechler P *et al.* Preventing mitochondrial fission impairs mitochondrial function and leads to loss of mitochondrial DNA. *PLoS One* 2008; **3**: e3257.
45. Wang DB, Garden GA, Kinoshita C, Wyles C, Babazadeh N, Sopher B *et al.* Declines in Drp1 and parkin expression underlie DNA damage-induced changes in mitochondrial length and neuronal death. *J Neurosci* 2013; **33**: 1357–1365.
46. Ishihara N, Nomura M, Jofuku A, Kato H, Suzuki SO, Masuda K *et al.* Mitochondrial fission factor Drp1 is essential for embryonic development and synapse formation in mice. *Nat Cell Biol* 2009; **11**: 958–966.
47. Horn SR, Thomenius MJ, Johnson ES, Freel CD, Wu JQ, Coloff JL *et al.* Regulation of mitochondrial morphology by APC/CCdh1-mediated control of Drp1 stability. *Mol Biol Cell* 2011; **22**: 1207–1216.
48. Singhal SS, Yadav S, Roth C, Singhal J. RLIP76: a novel glutathione-conjugate and multi-drug transporter. *Biochem Pharmacol* 2009; **77**: 761–769.
49. Awasthi YC, Sharma R, Cheng JZ, Yang Y, Sharma A, Singhal SS *et al.* Role of 4-hydroxynonenal in stress-mediated apoptosis signaling. *Mol Aspects Med* 2003; **24**: 219–230.
50. Paxinos G, Watson C. *The Rat Brain in Stereotaxic Coordinates.* 3rd edn. Academic Press: San Diego, CA, USA, 1997.
51. Kim JE, Kang TC. The P2 × 7 receptor-pannexin-1 complex decreases muscarinic acetylcholine receptor-mediated seizure susceptibility in mice. *J Clin Invest* 2011; **121**: 2037–2047.
52. Kim JE, Ryu HJ, Kim MJ, Kim DW, Kwon OS, Choi SY *et al.* Pyridoxal-5′-phosphate phosphatase/chronophin induces astroglial apoptosis via actin-depolymerizing factor/cofilin system in the rat brain following status epilepticus. *Glia* 2010; **58**: 1937–1948.

Supplementary Information accompanies this paper on Cell Death and Differentiation website (http://www.nature.com/cdd)